Available online at www.sciencedirect.com
ScienceDirect
Journal of Sound and Vibration 309 (2008) 507–528
JOURNAL OF SOUND AND VIBRATION
www.elsevier.com/locate/jsvi

Coupled horizontal and vertical bending vibrations of a stationary shaft with two cracks

A.C. Chasalevris, C.A. Papadopoulos*

Machine Design Laboratory, Department of Mechanical Engineering and Aeronautics, University of Patras, Patras-26504, Greece

Received 18 April 2006; received in revised form 12 July 2007; accepted 19 July 2007
Available online 14 September 2007

Abstract

This paper investigates the coupled bending vibrations of a stationary shaft with two cracks. It is known from the literature that, when a crack exists in a shaft, the bending, torsional, and longitudinal vibrations are coupled. This study focuses on the horizontal and vertical planes of a cracked shaft, whose bending vibrations are caused by a vertical excitation, in the clamped end of the model. When the crack orientations are not symmetrical to the vertical plane, a response in the horizontal plane is observed due to the presence of the cracks. The crack orientation is defined by the rotational angle of the crack, a parameter which affects the horizontal response. When more cracks appear in a shaft, then the coupling becomes stronger or weaker depending on the relative crack orientations. It is shown that a double peak appears in the vibration spectrum of a cracked or multi-cracked shaft.

Modeling the crack in the traditional manner, as a spring, yields analytical results for the horizontal response as a function of the rotational angle and the depths of the two cracks. A 2×2 compliance matrix, containing two non-diagonal terms (those responsible for the coupling) serves to model the crack. Using the Euler–Bernoulli beam theory, the equations for the natural frequencies and the coupled response of the shaft are defined. The experimental coupled response and eigenfrequency measurements for the corresponding planes are presented. The double peak was also experimentally observed.

1. Introduction

1.1. Modeling the crack with compliance matrix

In general, the local flexibility of a cracked beam can be described by the local flexibility matrix $\mathbf{C}$, whose dimension depends on the number of the degrees of freedom (dof) considered (maximum 6×6). Such a matrix was first introduced for beams of rectangular cross section with transverse surface cracks by Dimarogonas and Paipetis [1]. Some of the elements of this matrix were identified as direct compliances and have been computed previously by several authors. By inversion of the compliance matrix, the local stiffness matrix can be obtained as $\mathbf{K} = \mathbf{C}^{-1}$. The non-diagonal terms of the matrix show that a crack causes coupling between the longitudinal

*Corresponding author. Tel.: +30 261 096 9426; fax: +30 261 099 6258.
E-mail address: chris.papadopoulos@upatras.gr (C.A. Papadopoulos).

0022-460X/$ - see front matter © 2007 Elsevier Ltd. All rights reserved.
doi:10.1016/j.jsv.2007.07.039

and bending vibrations, between the lateral and torsional vibrations, and between the bending vibrations in two perpendicular planes.

Dimarogonas and Paipetis [1], introduced the full 5×5 flexibility matrix for the cracked region and computed the local flexibility for a rectangular beam with a transverse crack neglecting torsion. Furthermore, they observed that this matrix was not purely diagonal but had non-diagonal terms that indicated coupling between the longitudinal and lateral vibrations. Papadopoulos and Dimarogonas [2] and Papadopoulos [3] calculated the complete matrix $\mathbf{C}(6 \times 6)$ of the local compliance induced by the crack along with the non-diagonal terms of the matrix which show the directions in which coupling exists.

The local compliance in each direction is calculated using the strain energy release rate method and the associated stress intensity factor as given by Tada et al. [4]. Okamura et al. [5] and Liebowitz et al. [6,7] computed the diagonal element corresponding to tension. Rice and Levy [8] computed the tension-bending terms and their coupling; the torsion terms were computed by Dimarogonas and Massouros [9].

1.2. Coupled vibrations of cracked shafts

It is known that a crack in a structure can cause coupled vibrations. The coupled response is useful not only in proving the existence of a crack but also in identifying characteristics of the crack such as its depth and position. The usage of coupled responses is based on the fact that when a crack appears in a structure, the response of an excitation is observed not only in the direction of the excitation but also in other directions.

The coupling is strongly dependent on the position of the crack in the cross section. In other words, the coupling is affected by the ''amount'' of dissimilarity in moments of inertia in the cracked cross section. As the crack rotates following the rotation of the rotor, it passes across areas that increase or decrease the cracked cross-section asymmetry to the plane of excitation. In these areas, it is important to know the exact value of the local compliance matrix so as to predict precisely the coupling effect in the eigenfrequency and the response of the shaft. Darpe et al. [10] gave values of the compliance matrix as a function of the rotational angle of the crack.

In order to develop models able to identify the crack-induced coupling effect, many researchers have studied in detail the nonlinear phenomenon of crack breathing. To model the breathing of the crack, Grabowski [11] suggested a change in the stiffness between an uncracked rotor, representing the closed crack, and the cracked rotor, representing the open state of the crack at the particular rotor angular position where the crack edge becomes vertical. Alternatively, the change takes place when there is a change in the sign of the rotor response in a rotor-fixed coordinate in the crack direction (perpendicular to crack edge); this is referred to as the hinge model, introduced by Gasch [12] in 1976.

Later, Nelson and Nataraj [13] developed a finite element formulation of a crack element. They used a rotating stiffness variation that depended on the rotor curvature at the crack section. Mayes and Davies [14] suggested a sinusoidal stiffness variation in order to model the breathing in a more sensible way, since a rotor crack is expected to open and close gradually due to gravity. Papadopoulos and Dimarogonas [15–17] represented stiffness variation by way of a truncated, four-term series using known stiffness matrices corresponding to a fully open, a half-open–half-closed, and a fully closed crack. Schmalhorst [18] used contact segments on the face of the crack in a FE model to help decide which part of the crack face was under pressure and the resultant breathing behavior of the cracked part. Li et al. [19] represented the crack as a hinge of variable stiffness in two rotor-fixed lateral directions. The crack was introduced at the node of a finite element model (FEM). The stiffness change depended on the direction of the bending moment at the crack cross section. Wauer [20] replaced the local geometric discontinuity with a discontinuity in load and used Galerkin's method to obtain a response. The crack was assumed to be completely closed or completely open depending on the rotor curvature. Ostachowicz and Krawczuk [21] used a beam FEM with a modified stiffness matrix to account for the crack effect and consider all but the axial dof. They found a lateral response to torsional excitation for a rotating shaft with an open crack. Sekhar and Prabhu [22] used a FEM for the cracked rotor with an open crack and studied the possibility of backward whirl and bending stress fluctuations due to the crack. Abraham and Brandon [23] proposed a substructure approach for modeling the breathing behavior of the crack using Lagrange multipliers.

1.3. Multi-cracked shafts

A free vibration analysis model of multi-cracked shafts is presented for the first time by Tsai and Wang [24]. The Timoshenko beam theory is used and the cracks are assumed to remain opened. The effects of both relative distances along the axis and/or orientations of cracks are considered in the free vibration analysis.

The problem of multiple fatigue cracks in shafts could appear when multiple loads are applied. Sekhar [25] considered a FEM analysis on flexural vibrations of a rotor system by including two transverse open cracks. He noticed appreciable eigenfrequency changes for shafts having low slenderness ratios. In the case of two cracks of unequal depths, the larger crack has the more significant effect on the eigenfrequency and the effect of even small cracks on the stability speed is very much evident from the results.

Darpe et al. [26] studied the effect of the presence of two transverse surface cracks using the strain energy release concept. The flexibility of the cracked shaft due to two surface cracks having an angle γ between them is calculated. They presented the effect of the interaction of the two cracks on the breathing behavior and on the unbalance response of the rotor. The mutual position and orientation of the two cracks significantly changes the dynamic response of the rotor.

A model-based approach for two crack identification has been applied by Sekhar [27] in a rotor system. The fault-induced change in the rotor system is taken into account by equivalent loads in the mathematical model. The equivalent loads are virtual forces and moments acting on the linear undamaged system in such a way as to generate a dynamic behavior identical to the measured one in the damaged system. The rotor has been modeled using the finite element method, while the cracks are considered through local flexibility changes. The cracks have been identified by their depths and locations on the shaft.

Patil and Maiti [28] present an approximate method for detection of multiple open cracks using frequency measurements. The procedure gives a linear relationship explicitly between the changes in natural frequencies of the beam and the damage parameters. These parameters are determined from the knowledge of changes in the natural frequencies.

1.4. The present approach

In this paper, the values of the 2×2 compliance matrix are calculated for each angle of an entire rotation of the transverse crack. In the whole rotation, some rotation angles permit calculation of the compliance using the stress intensity factor of the crack, but some others prevent this because the stress intensity factor is not usable for any percentage of the crack depth. So, for cases where the crack depth makes the stress intensity factor unreliable, the compliance values are computed by interpolating between trustworthy compliance values. The interpolation areas are obtained using B-splines. At the same time, calculations determine the changes in the four terms of the compliance matrix that concern bending for an entire rotation.

The bending coupling effect as a function of rotational angle and depth of the crack is investigated and the results for the change in natural frequency and response are obtained and presented. The analytical results are compared with experimental response measurements in order to validate the theoretical model of coupled bending vibrations in a clamped-free shaft. The analytical model considers two cracks of different depths and rotational angles, while the experimental model considers a shaft with one crack. The fact that two cracks are introduced in the shaft aims at presenting that two cracks can cause more or less intense coupling depending at the angular position and the location of each other. There are cases in which the coupling is insensible even with two cracks present, but there are also cases in which one crack, even with small depth, can provoke the coupling phenomenon clearly. The experimental procedure aims at the demonstration of the coupling phenomenon in a clamped-free stationary shaft with coupling observed in the frequency response functions of both planes.

2. The compliance of the rotating crack

A Cartesian coordinate system ZOY is considered in Fig. 1, with point O in the center of the circular cross section. The angle φ defines the rotational position of the crack, taking values from 0° to 180° in order to cover all the rotational situations (compliance takes symmetrical or anti-symmetrical values for the other half).

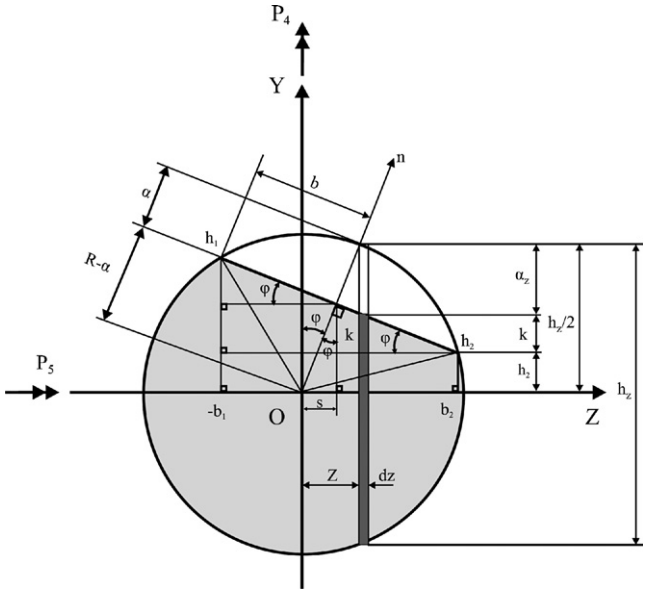

Fig. 1. The geometry of rotating crack section when $\varphi > 0$.

The bounds for the integration of Eqs. (3)–(6) are now from $-\zeta \times \bar{b}_1$ to $\zeta \times \bar{b}_2$ for the variable ζ as in Ref. [29], and from $(\bar{h}_2 + \bar{k})$ to $\sqrt{1-\bar{z}^2}$ for the variable y, defined as follows in Eqs. (1) and (2):

$$b_1 = b\cos\varphi - s, \quad b_2 = b\cos\varphi + s, \quad s = (R-a)\sin\varphi, \quad k = (b_2 - z)\sin\varphi, \tag{1}$$

$$h_1 = b\sin\varphi + (R-a)\cos\varphi, \quad h_2 = -b\sin\varphi + (R-a)\cos\varphi. \tag{2}$$

Here $\bar{h}_2 = h_2/R$, $\bar{k} = k/R$ and all variables in Eqs. (1) and (2) take dimensionless values (indicated by the same variable with a bar) when divided by R.

However $\zeta = 1$ for $\bar{a} = a/R \leqslant 1$, whereas for $\bar{a} > 1$, it is recommended a value of $\zeta = 0.95$ to be used [29]. The dimensionless local compliance contains only the variables $\bar{a}$ and φ, so if one defines $\bar{y}_1 = \bar{y} - 1 + \bar{a}$, and $\lambda_{\bar{y}} = \bar{y}_1/\bar{h}_z$, then the following double integrals for the compliance are obtained [30,31]:

$$\bar{c}_{55}(\bar{a},\varphi) = c_{55}(\bar{a},\varphi)\frac{ER^3}{1-\nu^2} = \frac{32}{\pi}\int_{-\zeta\bar{b}_1(\bar{a},\varphi)}^{\zeta\bar{b}_2(\bar{a},\varphi)}\int_{\bar{k}+\bar{h}_2}^{\sqrt{1-\bar{z}^2}}(1-\bar{z}^2)\bar{y}_1 F_2^2(\lambda_{\bar{y}})\,\mathrm{d}\bar{y}\,\mathrm{d}\bar{z}, \tag{3}$$

$$\bar{c}_{44}(\bar{a},\varphi) = c_{44}(\bar{a},\varphi)\frac{ER^3}{1-\nu^2} = \frac{16}{\pi}\int_{-\zeta\bar{b}_1(\bar{a},\varphi)}^{\zeta\bar{b}_2(\bar{a},\varphi)}\int_{\bar{k}+\bar{h}_2}^{\sqrt{1-\bar{z}^2}}\bar{z}^2\bar{y}_1 F_1^2(\lambda_{\bar{y}})\,\mathrm{d}\bar{y}\,\mathrm{d}\bar{z}, \tag{4}$$

$$\bar{c}_{45}(\bar{a},\varphi) = c_{45}(\bar{a},\varphi)\frac{ER^3}{1-\nu^2} = \frac{32}{\pi}\int_{0}^{\zeta b_2(\bar{a},\varphi)}\int_{\bar{k}+\bar{h}_2}^{\sqrt{1-\bar{z}^2}}\bar{z}\bar{y}_1\sqrt{1-\bar{z}^2}F_1(\lambda_{\bar{y}})F_2(\lambda_{\bar{y}})\,\mathrm{d}\bar{y}\,\mathrm{d}\bar{z}, \tag{5}$$

$$\bar{c}_{45}(\bar{a},\varphi) = c_{45}(\bar{a},\varphi)\frac{ER^3}{1-\nu^2} = c_{54}(\bar{a},\varphi)\frac{ER^3}{1-\nu^2} = \bar{c}_{54}(\bar{a},\varphi). \tag{6}$$

The rotation of the crack is an important issue that strongly affects the coupling phenomenon. Under the steady bending load in the vertical direction, the crack opens and closes as a function of its rotational angle.

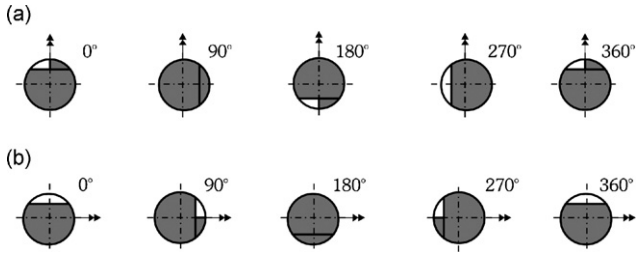

Fig. 2. The breathing of the crack for (a) horizontal load and (b) vertical load.

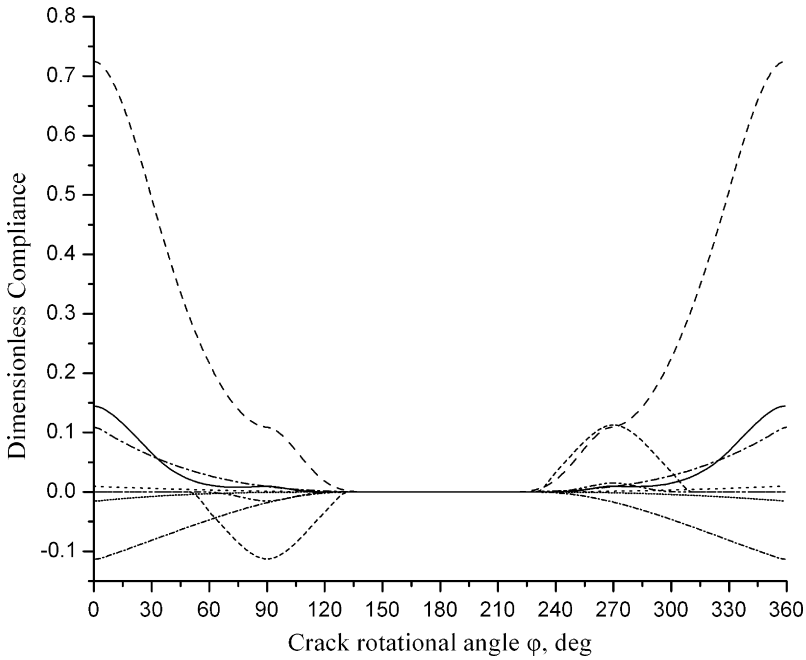

Fig. 3. Dimensionless compliances $\bar{c}_{44}$,$\bar{c}_{45}$,$\bar{c}_{54}$ and $\bar{c}_{55}$as a function of rotational angle for crack depths $\bar{a} = 0.2$ and 0.4. Continuous line: $\bar{c}_{55}$ for $\bar{a} = 0.2$; dashed line: $\bar{c}_{55}$ for $\bar{a} = 0.4$; dotted line: $\bar{c}_{44}$ for $\bar{a} = 0.2$; dashed-dotted line: $\bar{c}_{44}$ for $\bar{a} = 0.4$; dashed-dotted line: $\bar{c}_{45}$ for $\bar{a} = 0.2$; short dashed line: $\bar{c}_{45}$ for $\bar{a} = 0.4$; short dotted line: $\bar{c}_{54}$ for $\bar{a} = 0.2$; and short dashed-dotted line: $\bar{c}_{54}$ for $\bar{a} = 0.4$.

When the bending load is horizontal, the opening and closing of the crack occurs in different rotational angles than those for a vertical load. In Figs. 2a and b, the opening and closing of the crack for both loads is shown as a function of the rotational angle. In these two situations of the bending load, there are similar conditions for the crack (opened, closed, semi-open). The value of any compliance for the rotational angles shown in Fig. 2 for a region encompassing $\varphi = \pm 30^{\circ}$ is computed using Eqs. (3)–(6). For the remaining rotational angles, each compliance function is calculated by interpolating the known values using B-splines as in Refs. [30,32]. The change of each compliance as a function of the rotational angle and depth of the crack is presented in Fig. 3. Another way to calculate the compliance function could be by computing the compliance normal to the crack edge and expressing it along the vertical and horizontal direction. This approach is used by many researchers in this field, and results in a harmonic periodic compliance change. However, the compliance change is not exactly harmonic, since it has some constant areas during rotation (when the crack is closed) but it is, of course, periodic. In the present approach the compliance is calculated in each angle of rotation of the shaft giving reliable values.

Importantly, there are rotational angles for which any compliance can be equal to zero. Compliance $\bar{c}_{55}$ is equal to zero for the rotational angles that close completely the crack. The same goes for compliance $\bar{c}_{44}$.

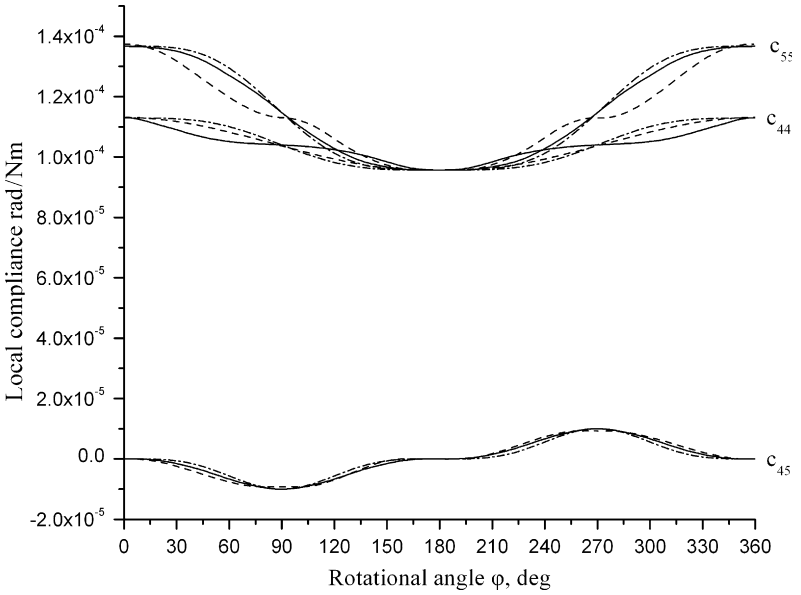

Fig. 4. Comparison of three different approaches (continuous line: A.K. Darpe et al.; dashed dot line: Dimarogonas and Papadopoulos; and dashed line: current approach) for local compliances C_{55} and C_{45} as a function of rotational angle φ.

Compliance $\bar{c}_{45}$ takes a value equal to zero not only for a completely closed crack but also for those rotational angles where the crack is symmetric to the plane of the bending load. So, $\bar{c}_{45}(0) = \bar{c}_{45}(180) = 0$. In Fig. 4, the current and traditional approaches for the compliance change during crack rotation are compared with a truncated cosine series in Ref. [15] and a recent approach made in Ref. [10].

3. Coupled bending vibrations of the shaft using Euler–Bernoulli theory

Consider a clamped-free stationary shaft of length L with two transverse cracks of depth α_1 and α_2 at distances L_1 and L_2, respectively, from the clamped end. A Cartesian coordinate system is defined as in Fig. 5; the vertical plane OXY is defined as plane 5 and the horizontal plane OXZ is defined as plane 4. The bending vibrations occur in both planes under excitation in plane 5. The cracks divide the shaft into three parts with vertical displacements $Y_i(x,t)$, $i = 1,2,3$ and horizontal displacements $Z_i(x,t)$, $i = 1,2,3$ as shown in Fig. 5. Each part is connected with the next by the spring K_i, whose magnitude depends on the crack depth and the crack angular position. The magnitude of K_i is different for the vertical and horizontal plane. The three parts of the shaft vibrate in the vertical plane (plane 5) with $Y_1(x,t)$, $Y_2(x,t)$, and $Y_3(x,t)$, and in the horizontal plane (plane 4) with $Z_1(x,t)$, $Z_2(x,t)$, and $Z_3(x,t)$. When there is no crack, the shaft is considered to vibrate independently in two planes. In this case, the response exists exclusively in the plane of excitation. So, the equations of motion as shown below are not coupled (as happens in rotating shafts).

The bending moment P_5 is applied at the free end. The bending vibration is described by the Euler–Bernoulli equations, in dimensionless form, for the vertical and horizontal plane as follows:

$$-\frac{\partial^4 \bar{Y}_i}{\partial \bar{x}^4} = \frac{1}{\bar{C}_y^2}\frac{\partial^2 \bar{Y}_i}{\partial \tau^2}, \quad -\frac{\partial^4 \bar{Z}_i}{\partial \bar{x}^4} = \frac{1}{\bar{C}_z^2}\frac{\partial^2 \bar{Z}_i}{\partial \tau^2}, \quad \text{where} \quad \begin{array}{ll} \text{for } i=1, & 0 \leqslant \bar{x} \leqslant \bar{L}_1, \\ \text{for } i=2, & \bar{L}_1 < \bar{x} \leqslant \bar{L}_2, \\ \text{for } i=3, & \bar{L}_2 < \bar{x} \leqslant 1. \end{array} \tag{7}$$

Here $i = 1,2,3$ is the part of the beam, $\bar{x} = x/L$, $\bar{Y}_i = Y_i/L$, $\bar{Z}_i = Z_i/L$, $\tau = t/T$ is the dimensionless time, T is the period of vibration, $\bar{C}_y = \bar{C}_z = \sqrt{EI/\mu}(T/L^2)$, $\mu = A\rho$ is the linear density, $\rho = 7860\,\mathrm{kg\,m^{-3}}$ is the density of the material, $A = \pi R^2$ is the entire cross-section area of the shaft, $I = \pi R^4/4$ is the moment of inertia

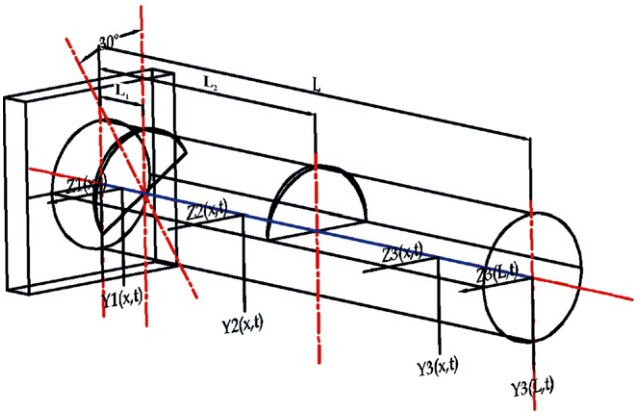

Fig. 5. A shaft with two cracks.

of the entire cross-section area of the shaft, $E = 210\,\text{GPa}$ is the Young's modulus of elasticity, and R is the shaft radius.

After the separation of variables, the three partial solutions for each part of the vertical plane are in dimensionless form:

$$\bar{Y}_1(\bar{x}) = A_1\cosh(\bar{k}_y\bar{x}) + A_2\sinh(\bar{k}_y\bar{x}) + A_3\cos(\bar{k}_y\bar{x}) + A_4\sin(\bar{k}_y\bar{x}), \tag{9}$$

$$\bar{Y}_2(\bar{x}) = A_5\cosh(\bar{k}_y\bar{x}) + A_6\sinh(\bar{k}_y\bar{x}) + A_7\cos(\bar{k}_y\bar{x}) + A_8\sin(\bar{k}_y\bar{x}), \tag{10}$$

$$\bar{Y}_3(\bar{x}) = A_9\cosh(\bar{k}_y\bar{x}) + A_{10}\sinh(\bar{k}_y\bar{x}) + A_{11}\cos(\bar{k}_y\bar{x}) + A_{12}\sin(\bar{k}_y\bar{x}). \tag{11}$$

The three partial solutions for each part of the horizontal plane are:

$$\bar{Z}_1(\bar{x}) = B_1\cosh(\bar{k}_z\bar{x}) + B_2\sinh(\bar{k}_z\bar{x}) + B_3\cos(\bar{k}_z\bar{x}) + B_4\sin(\bar{k}_z\bar{x}), \tag{12}$$

$$\bar{Z}_2(\bar{x}) = B_5\cosh(\bar{k}_z\bar{x}) + B_6\sinh(\bar{k}_z\bar{x}) + B_7\cos(\bar{k}_z\bar{x}) + B_8\sin(\bar{k}_z\bar{x}), \tag{13}$$

$$\bar{Z}_3(\bar{x}) = B_9\cosh(\bar{k}_z\bar{x}) + B_{10}\sinh(\bar{k}_z\bar{x}) + B_{11}\cos(\bar{k}_z\bar{x}) + B_{12}\sin(\bar{k}_z\bar{x}). \tag{14}$$

Here $\bar{k}_y^2 = \omega/\omega_0$, $\bar{k}_z^2 = \omega/\omega_0$, ω is the vibration frequency and $\omega_0^2 = EI/(\mu L^4)$.

3.1. Boundary conditions and the characteristic determinant

There are 24 unknown variables in the above equations, A_i and B_i, $i = 1$–12, and the solution for the equations of motion can be calculated using 24 boundary conditions (BC), 12 for each plane. In Table 1 these BCs are presented in dimensionless form. The boundary conditions are similar for both planes. In equations of Table 1, c_{ij_1} and c_{ij_2} ($i = 4,5$ and $j = 4,5$) are the local compliances of the first and second crack, correspondingly, and they are defined as

$$c_{ij} = \frac{(1-\nu^2)}{ER^3}\bar{c}_{ij}. \tag{15}$$

Table 1
Boundary conditions for a clamped-free shaft with a crack in the two main directions of vibration

Dimensionless BC of vertical vibration	Dimensionless BC of horizontal vibrations
$\bar{Y}_1(0)=0$	$\bar{Z}_1(0)=0$
$\bar{Y}'_1(0)=0$	$\bar{Z}'_1(0)=0$
$\bar{Y}''_3(1)=0$	$\bar{Z}''_3(1)=0$
$\bar{Y}'''_3(1)=0$	$\bar{Z}'''_3(1)=0$
$\bar{Y}_1(\bar{L}_1)=\bar{Y}_2(\bar{L}_1)$	$\bar{Z}_1(\bar{L}_1)=\bar{Z}_2(\bar{L}_1)$
$\bar{Y}''_1(\bar{L}_1)=\bar{Y}''_2(\bar{L}_1)$	$\bar{Z}''_1(\bar{L}_1)=\bar{Z}''_2(\bar{L}_1)$
$\bar{Y}'''_1(\bar{L}_1)=\bar{Y}'''_2(\bar{L}_1)$	$\bar{Z}'''_1(\bar{L}_1)=\bar{Z}'''_2(\bar{L}_1)$
$\frac{\pi R}{4L}(1-\nu^2)(\bar{c}_{55_1}\bar{Y}''_1(\bar{L}_1)+\bar{c}_{54_1}\bar{Z}''_1(\bar{L}_1))=\Delta\bar{Y}'_{21}(\bar{L}_1)$	$\frac{\pi R}{4L}(1-\nu^2)(\bar{c}_{44_1}\bar{Z}''_1(\bar{L}_1)+\bar{c}_{45_1}\bar{Y}''_1(\bar{L}_1))=\Delta\bar{Z}'_{21}(\bar{L}_1)$
$\bar{Y}_2(\bar{L}_2)=\bar{Y}_3(\bar{L}_2)$	$\bar{Z}_2(\bar{L}_2)=\bar{Z}_3(\bar{L}_2)$
$\bar{Y}''_2(\bar{L}_2)=\bar{Y}''_3(\bar{L}_2)$	$\bar{Z}''_2(\bar{L}_2)=\bar{Z}''_3(\bar{L}_2)$
$\bar{Y}'''_2(\bar{L}_2)=\bar{Y}'''_3(\bar{L}_2)$	$\bar{Z}'''_2(\bar{L}_2)=\bar{Z}'''_3(\bar{L}_2)$
$\frac{\pi R}{4L}(1-\nu^2)(\bar{c}_{55_2}\bar{Y}''_2(\bar{L}_2)+\bar{c}_{54_2}\bar{Z}''_2(\bar{L}_2))=\Delta\bar{Y}'_{32}(\bar{L}_2)$	$\frac{\pi R}{4L}(1-\nu^2)(\bar{c}_{44_2}\bar{Z}''_2(\bar{L}_2)+\bar{c}_{45_2}\bar{Y}''_2(\bar{L}_2))=\Delta\bar{Z}'_{32}(\bar{L}_2)$

Eqs. (9)–(14) are substituted into the 24 BC of Table 1 to obtain the homogenous system of 24 equations and 24 unknowns ($A_1,A_2,\ldots,A_{12}$ and $B_1,B_2,\ldots,B_{12}$) as follows:

$$[\mathbf{P}]\underbrace{\left\{\begin{array}{cccccccccc}A_1 & A_2 & \cdots & A_{12} & B_1 & B_2 & \cdots & B_{12}\end{array}\right\}^{\mathrm{T}}}_{24}=\underbrace{\left\{\begin{array}{cccc}0 & 0 & \cdots & 0\end{array}\right\}^{\mathrm{T}}}_{24}. \tag{16}$$

In Table 1, $\Delta\bar{Y}_{ij}=\bar{Y}_j-\bar{Y}_i$, $\Delta\bar{Z}_{ij}=\bar{Z}_j-\bar{Z}_i$, where $i=2,3$ and $j=1,2$ and $\bar{L}_i=L_i/L$, where $i=1,2$.

The characteristic determinant of the homogenous system in Eq. (16), $\det|\mathbf{P}|$, must be equal to zero for a non-trivial solution. The roots of the characteristic Eq. (17) are the eigenfrequencies of the multi-cracked shaft

$$\det|\mathbf{P}|=\det\begin{vmatrix}\mathbf{A} & \mathbf{B}\\ \mathbf{C} & \mathbf{D}\end{vmatrix}=0, \tag{17}$$

The sub-matrices **A**–**D**, included in Eq. (17), are defined in Appendix A.

3.2. Calculation of the eigenfrequencies of the multi-cracked shaft

Considering a shaft with two cracks of any characteristics (position, depth, rotational angle) the dimensionless compliances $\bar{c}_{55}$, $\bar{c}_{44}$, $\bar{c}_{54}$, $\bar{c}_{45}$ can be computed for both cracks and the characteristic determinant becomes a function of frequency ω. As seen in Section 2, there are areas of rotational angle in which the dimensionless compliances are equal to zero. The physical explanation of zero compliance is that the crack does not introduce any additional slope in the shaft in a specific direction, and so the term of the additional slope due to coupling in the boundary conditions of Table 1 becomes equal to zero. The same goes for the other terms that contain the dimensionless compliances $\bar{c}_{55}$ and $\bar{c}_{44}$.

For a shaft of $R/L=0.01$, and with two cracks at positions $\bar{L}_1=0.1$ and $\bar{L}_2=0.4$, variable depths $\bar{a}_1=\bar{a}_2=0.2,\ 0.4,\ 0.5,\ 0.6,\ 0.8$ and rotational angles $\varphi_1=\varphi_2=0^\circ$, the roots of characteristic determinant are presented in Table 2. The eigenfrequency change of a shaft with two cracks of constant depth and variable rotational angle are examined. Suppose the shaft has two cracks with depths $\bar{a}_1=\bar{a}_2=0.4$ and variable rotational angles $\varphi_1=\varphi_2=0^\circ, 30^\circ, 60^\circ, 90^\circ, 120^\circ, 150^\circ, 180^\circ$. The eigenfrequency change is shown in Table 3. As the crack rotational angle approaches 180°, the crack is fully closed and remains closed during the normal

Table 2
Variation of 1st, 2nd, and 3rd dimensionless eigenfrequencies of both planes vs. the crack depth when $\varphi_1 = \varphi_{12} = 90^\circ$

Crack depth	1st eigenfrequency	2nd eigenfrequency	3nd eigenfrequency
$\alpha_1/D = \alpha_2/D$	Vertical/horizontal		
0.0	3.516/3.516	22.035/22.035	61.700/61.700
0.1	3.509/3.515	22.000/22.034	61.660/61.697
0.2	3.482/3.511	21.896/22.015	61.527/61.674
0.25	3.458/3.504	21.800/21.988	61.410/61.642
0.3	3.427/3.493	21.671/21.941	61.253/61.583
0.4	3.337/3.440	21.287/21.724	60.796/61.317

Table 3
Variation of 1st, 2nd, and 3rd dimensionless eigenfrequencies of both planes vs. the rotational angle of the crack and for $\bar{a}_1 = \bar{a}_2 = 0.4$

Rotational angle (deg)	1st eigenfrequency	2nd eigenfrequency	3rd eigenfrequency
$\varphi_1 = \varphi_2$	Vertical/horizontal		
0	3.482/3.511	21.896/22.015	61.527/61.674
30	3.483/3.512	21.902/22.016	61.534/61.677
60	3.497/3.513	21.957/22.023	61.602/61.684
90	3.511/3.515	22.012/22.031	61.671/61.695
120	3.514/3.516	22.026/22.034	61.689/61.698
150	3.516/3.516	22.035/22.035	61.700/61.700
180	3.516/3.516	22.035/22.035	61.700/61.700

mode vibration because of the vertical static load. Thus, the eigenfrequency approaches the corresponding value of the uncracked shaft in Table 3.

3.3. Calculation of the coupled response of the multi-cracked shaft

The responses in the horizontal and vertical planes are given in Eqs. (9)–(14). The constants A_i, B_i with $i = 1,2,\ldots,12$ are obtained by the solution of the homogenous system as follows:

$$[\mathbf{P}]\underbrace{\left\{ A_1 \quad A_2 \quad \cdots \quad A_{12}\, B_1 \quad B_2 \quad \cdots \quad B_{12} \right\}^{\mathrm{T}}}_{24} = \underbrace{\left\{ 0 \quad 0 \quad \cdots \quad 0 \right\}^{\mathrm{T}}}_{24}. \tag{18}$$

Supposing two cracks with depths $\bar{a}_1 = \bar{a}_2 = 0.4$ in positions $\bar{L}_1 = 0.1$ and $\bar{L}_2 = 0.4$ and rotational angles $\varphi_1 = \varphi_2 = 0^\circ$, the dimensionless compliances take the following values from Fig. 3:

$$\bar{c}_{55_1} = \bar{c}_{55_2} = 0.72414, \quad \bar{c}_{44_1} = \bar{c}_{44_2} = 0.10906, \quad \bar{c}_{45_1} = \bar{c}_{45_2} = 0, \quad \bar{c}_{54_1} = \bar{c}_{54_2} = -0.11004.$$

When the vertical excitation in the clamped end exists, the system of Eq. (18) takes the form as follows:

$$[\mathbf{P}]\underbrace{\{ A_1 \quad A_2 \quad \cdots \quad A_{12}\, B_1 \quad B_2 \quad \cdots \quad B_{12} \}^{\mathrm{T}}}_{24} = \underbrace{\{ 0.0001 \quad 0 \quad \cdots \quad 0 \}^{\mathrm{T}}}_{24}. \tag{19}$$

The fact that $\bar{c}_{45_1} = \bar{c}_{45_2} = 0$ means that if a load is applied in plane 5 (the vertical plane), a coupling response does not exist in plane 4 (the horizontal plane). The vertical load exists in this example by setting $\bar{Y}_1(0) = 0.0001$, so after the system solution the variables B_i must be equal zero in order to have no horizontal response. Consider matrix **C**, the lower-left sub-matrix of **P** (see Appendix A). All of its terms contain the coupling dimensionless compliances $\bar{c}_{45_1}$ and $\bar{c}_{45_2}$, which are equal to zero. So, the terms with the zero compliance in the denominator are written off and matrix **C** is a zero matrix, indicating that there is no

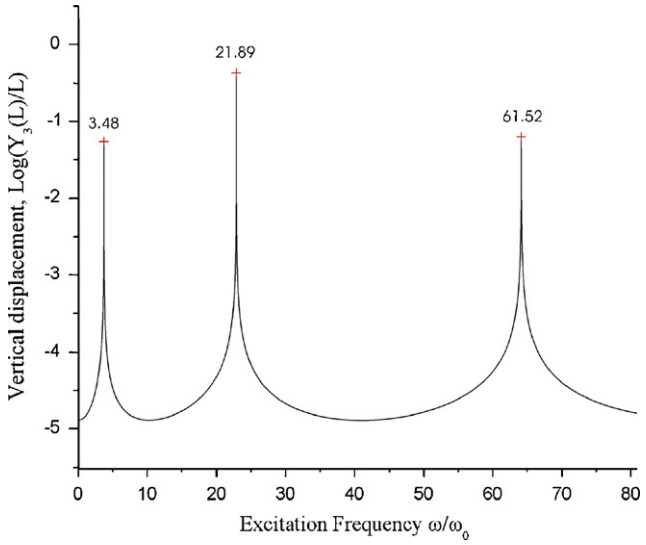

Fig. 6. Vertical response at the free end of the cracked shaft as a function of excitation frequency.

coupling from plane 5 to plane 4. When sub-matrix **B** is the zero matrix because of the zero values in compliances $\bar{c}_{54_1}$ and $\bar{c}_{54_2}$, then there is no coupling from plane 4 to plane 5. This happens when the cracks are totally closed. In this example, both cracks are symmetric in the vertical plane ($\varphi_1 = \varphi_2 = 0^\circ$) such that $\bar{c}_{45_1} = \bar{c}_{45_2} = 0$. Note that the frequency of the excitation changes from zero up to $\omega = 5000\,\mathrm{rad\,s^{-1}}$, indicating that the vibration passes through the first three resonances in the corresponding eigenfrequencies.

In Fig. 6, the vertical response is shown while the horizontal response is zero for any excitation frequency. As expected the resonance (maximum response) exists in the frequencies of Table 2. If both cracks are rotated equally such that $\varphi_1 = \varphi_2 = 90^\circ$, the compliances calculated are equal to $\bar{c}_{55_1} = \bar{c}_{55_2} = 0.10906$, $\bar{c}_{44_1} = \bar{c}_{44_2} = 0.0308$,$\bar{c}_{45_1} = \bar{c}_{45_2} = -0.11004$ and $\bar{c}_{54_1} = \bar{c}_{54_2} = -0.00563$. All other characteristics (depth, position) remain the same as in the previous case. In this example, the coupling phenomenon is observed in all resonances of the spectrum. In Fig. 7a, the horizontal eigenfrequency intrudes into the vertical spectrum by adding a characteristic peak in the frequency of $\omega/\omega_0 = 3.515$, which is the horizontal eigenfrequency as shown in Table 2. The same goes for the horizontal spectrum where the vertical eigenfrequency intrudes into it and generates the additional peak in Fig. 7b for $\omega/\omega_0 = 3.510$. The same phenomenon was also observed for any other eigenfrequency. Tables 2 and 3 show a low eigenfrequency shift. The practical significance for condition monitoring or diagnosis does not come up. However, there are geometric shaft models of smaller slenderness ratios that can cause greater flexural moments in the cracked section, so as to generate a more intense crack effect and a greater frequency shift.

As the crack depth increases, the coupling phenomenon becomes stronger and the eigenfrequencies of the two planes further diverge. In continuing, the response in both planes is calculated for different rotational angles of the cracks. In order to observe which amplitude dominates the other, the horizontal and vertical amplitudes in the free end are divided to define the amplitude ratio (AR) as $\mathrm{AR} = |Z_3(L)|/|Y_3(L)|$ with $\mathrm{AR} \in [0,1)$. The AR does take values near zero since the coupling effect cannot introduce vibrations of amplitudes as large as the amplitude of vibration in the plane of excitation. The AR shows that, for specific rotational angles, the horizontal vibration is zero while, at other rotational angles, there is a generation of horizontal vibrations that remain at very low amplitude with respect to those of the vertical plane. Note that the excitation exists only in the vertical plane. The vertical response does not significantly change during crack rotation; this is due to the fact that the excitation is in the same plane and so the crack breathing cannot affect a response that is due to an excitation in the same plane. On the other hand, the crack breathing produces a significant change in this response due to the coupling effect and not due to the excitation of this plane. The same phenomenon appears for the case of uniquely horizontal excitation. Fig. 8 shows that for 5 different excitation frequencies, the maximum coupling always exists in the rotational angle of 90°, which should be

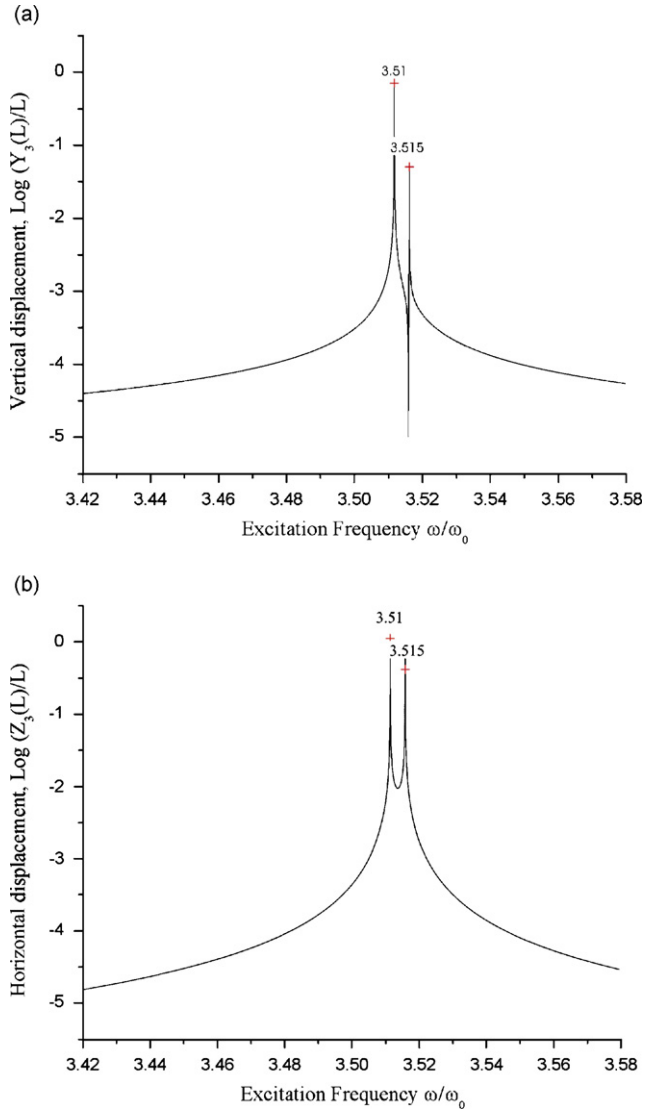

Fig. 7. (a) Vertical and (b) horizontal response in first resonance of Fig. 6.

obvious because of the maximization of the coupling local compliance. Note that the excitation frequencies are chosen to be different from those near resonance, because the resonance event causes unpredictable variations of vibration amplitudes in both planes.

Another numerical example includes a clamped-free shaft of $R/L = 0.05$. The slenderness ratio $2L/R = 40$, compared to the previous example, offers higher eigenfrequencies and, as a result, a greater absolute eigenfrequency shift due to the crack. Both crack depths are equal to $\bar{a}_1 = \bar{a}_2 = 0.8$. The cracks are located at the same point $\bar{L}_1 = \bar{L}_2 = 0.1$ at rotational angles $\varphi_1 = 90^\circ$ and $\varphi_2 = 270^\circ$. The local compliances for these characteristics are calculated as

$$\bar{c}_{55_1} = 1.6590, \quad \bar{c}_{44_1} = 0.5530, \quad \bar{c}_{45_1} = -1.0045, \quad \bar{c}_{54_1} = -0.08,$$
$$\bar{c}_{55_2} = 1.6590, \quad \bar{c}_{44_2} = 0.5530, \quad \bar{c}_{45_2} = 1.0045, \quad \bar{c}_{54_2} = -0.08.$$

Both cracks are symmetric with respect to the center of the cracked cross section and the aim of this acceptance is to show that no coupling exists when the cracked section is symmetric with respect to the plane

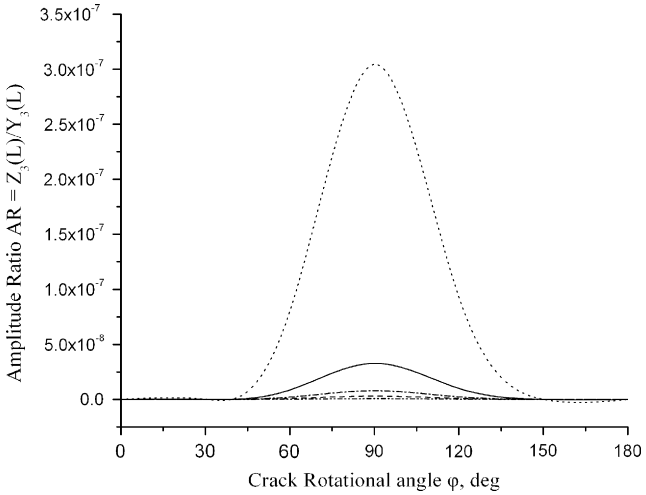

Fig. 8. The amplitude ratio as a function of rotational angle for 5 different values of excitation frequency (dash: $\omega = 10$ rad/s, continuous: $\omega = 90$ rad/s, short dash: $\omega = 250$ rad/s, dash dot: $\omega = 500$ rad/s, dash dot dot: $\omega = 800$ rad/s).

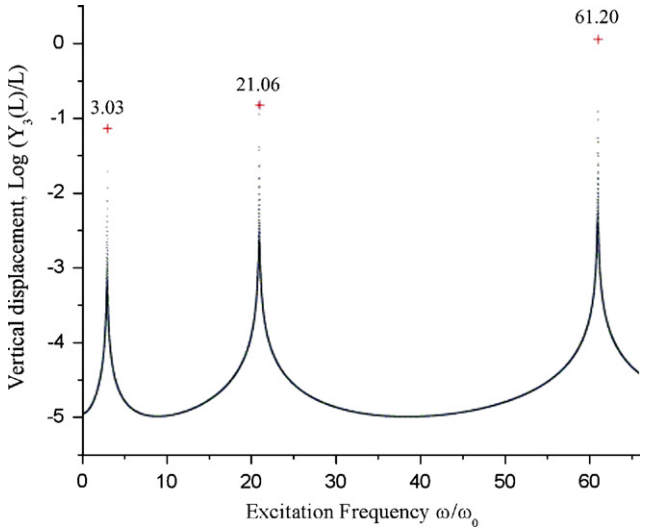

Fig. 9. No coupling exists when the cracks are located symmetrically to the vertical plane and at the same location, $\bar{a}_1 = \bar{a}_2 = 0.8, \bar{L}_1 = \bar{L}_2 = 0.1$, and $\varphi_1 = 90^\circ$, $\varphi_2 = 270^\circ$.

of the load even with two cracks present. The vertical response in Fig. 9 has no additional peaks due to coupling while the horizontal response is zero.

If the second crack is moved at $\bar{L}_2 = 0.2$ then, due to the difference in bending moment in each cracked section, a coupling exists and the vertical and horizontal response obtain additional peaks. In Fig. 10 only the vertical response of the coupled vibration is presented. It is easy to show that, when the orientations of both cracks are the same, the coupling becomes more obvious.

There is also a case in which the coupling exists one-way. To explain further, if one of the two coupling compliances $\bar{c}_{45}$, $\bar{c}_{54}$ is equal to or even near to zero, then the coupling exists only from one plane to the other. For example, if $\bar{c}_{45} \to 0$ then the coupling exists from the horizontal to the vertical plane while the coupling in the inverse direction is not observed. Also if $\bar{c}_{54} \to 0$, then only the coupling from the vertical to the horizontal plane is presented. For $\bar{a}_1 = \bar{a}_2 = 0.4$ there are crack rotational angles, such as $\varphi_1 = \varphi_2 = 130^\circ$ that give

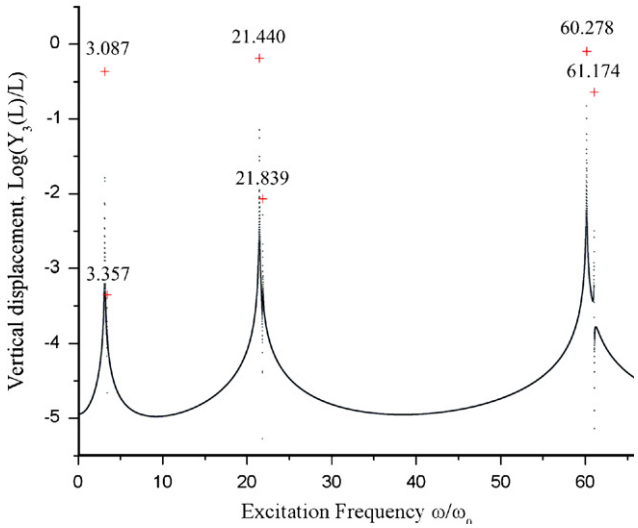

Fig. 10. Coupling existing in the vertical response of the shaft, when cracks are located symmetrically to the vertical plane and at different location, $a_1/R = a_2/R = 0.8$, $L_1 = 0.1L$, $L_2 = 0.2l$, and $\varphi_1 = 90$, $\varphi_2 = 270^\circ$.

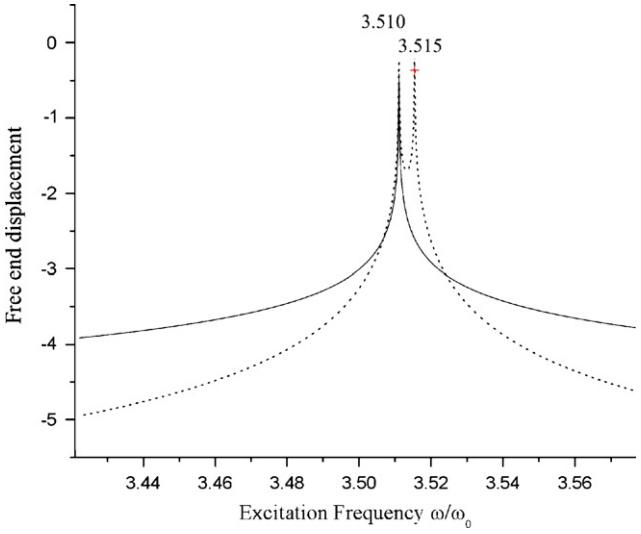

Fig. 11. The first resonance in vertical (continuous line) and horizontal (dashed line) plane for the case that $\bar{c}_{54_1} = \bar{c}_{54_2} = 0$. Coupling exists only in the horizontal plane.

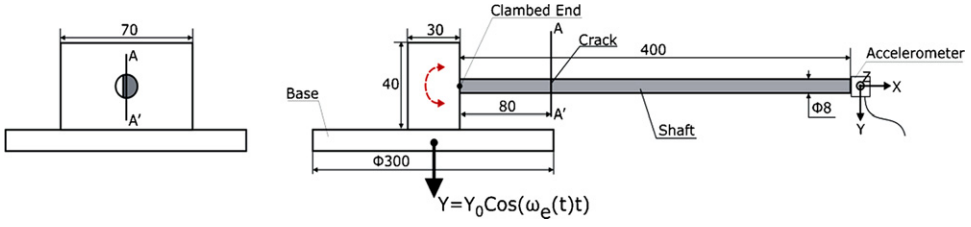

Fig. 12. The experimental model: clamped-free shaft with a cut in $\varphi_1 = 90^\circ$.

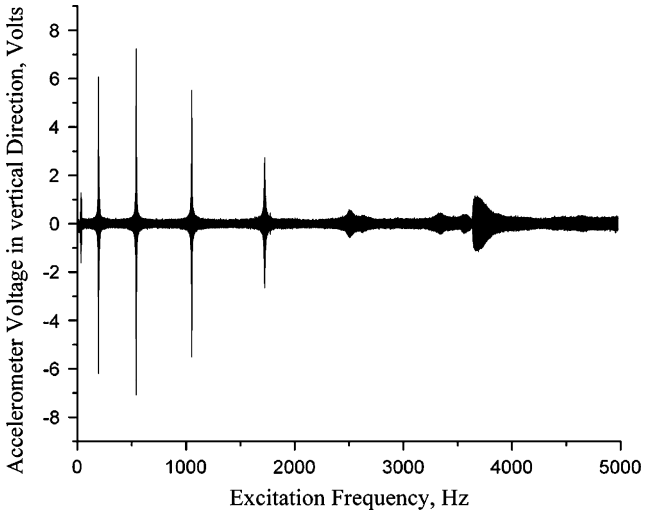

Fig. 13. Experimental measurements of the vertical acceleration at the free end of the intact shaft as a function of excitation frequency.

Table 4
Experimental measurement of the double resonance peak, due to the coupling, in the two main planes, for the 1st, 2nd and 3rd eigenfrequency, as a function of cut depth calculated in the experimental model

Cut depth	$\alpha/D=0.0$	$\alpha/D=0.1$	$\alpha/D=0.2$	$\alpha/D=0.4$
Peak	1st/2nd			
Vertical plane				
1	30.0/30.0	29.5/29.5	30.0/30.0	29.8/29.8
2	192.2/196.9	191.5/196.5	190.7/195.2	189.5/193.9
3	538.5/547.4	537.8/546.4	537.6/546.1	536.5/545.6
Horizontal plane				
1	30.0/30.0	29.5/29.5	29.6/29.6	29.6/29.6
2	192.3/196.8	191.6/196.4	190.8/195.1	189.6/193.8
3	538.5/546.1	538.4/545.8	537.7/545.5	536.8/545.1

compliance values:

$$\bar{c}_{55_1}=\bar{c}_{55_2}=0.01704,\quad \bar{c}_{44_1}=\bar{c}_{44_2}=0.00315,\quad \bar{c}_{45_1}=\bar{c}_{45_2}=-0.0279,\quad \bar{c}_{54_1}=\bar{c}_{54_2}=0.$$

The frequency response for crack positions $\bar{L}_1=0.1$ and $\bar{L}_2=0.2$ obtains double peaks only in the horizontal plane while, in vertical plane, no coupling is introduced, as it is shown in Fig. 11 for the first resonance frequency. Same results are obtained but not presented for any other resonance frequency.

4. Experimental evidence

In order to observe and validate the theoretical model of the coupled bending vibrations, an experiment was carried out. A clamped-free shaft with one cut was vibrated using a vertical excitation that is transferred to the clamped end of the shaft using the base as shown in Fig. 12. The excitation frequency was a function of time $\omega_e(t)=10t$, $0<t<500$ s with a maximum value of 5000 Hz so as to pass through the seventh resonance frequency of the beam. Using an accelerometer in the free end of the beam, two signals, the vertical and the horizontal accelerations were acquired in the free end. The accelerometer had an insignificant weight with respect to the shaft, and so it was not accounted for in the analytical procedure. The signals for vertical and horizontal acceleration, in the free end of the intact shaft, are acquired and in Fig. 13 the vertical one is presented.

Table 5
Analytical calculation of the double resonance peak, due to the coupling, in the two main planes, for the 1st, 2nd and 3rd eigenfrequency, as a function of crack depth

Crack depth	$\alpha/D = 0.0$	$\alpha/D = 0.1$	$\alpha/D = 0.2$	$\alpha/D = 0.4$
Double peak	1st/2nd			
Vertical plane				
1	30.00/30.00	30.00/30.00	29.98/29.99	29.74/29.93
2	196.71/196.71	196.70/196.70	196.70/196.70	196.58/196.67
3	565.64/565.64	565.61/565.63	565.33/565.60	561.27/564.38
Horizontal plane				
1	30.00/30.00	30.00/30.00	29.98/30.00	29.74/29.93
2	196.71/196.71	196.70/196.70	196.70/196.70	196.58/196.67
3	565.64/565.64	565.61/565.63	565.33/565.60	561.27/564.38

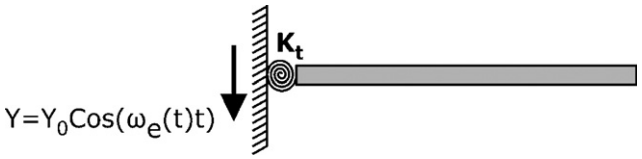

Fig. 14. The torsional spring at the clamped end of the shaft.

A crack is very different from a slot [33,34], but the comparison between the analytical results of the cracked shaft and the experimental results of a slotted shaft can be justified because, cracks, as well as slots, cause coupling at some rotational angles. This procedure focused on investigating the response due to coupling that is provoked either from cracks or slots, so long as greater depths in both defects intensively affect the coupling. An eigenfrequency shift between the two cases is prospective.

The basic difference between a cracked and a slotted shaft is that the slotted one does not ''breathe'' and remains open during the rotation. A second difference is that the stress intensity factor of the slotted shaft should be different from that of the crack, because the radius of the crack tip tends to zero since the radius of the slot depends on the radius of the saw used to open the slot. The calculation of the stress intensity factor depends on the applied loads and the geometry (depth and width) of the crack.

The common property, that both slotted and cracked shafts have, is the shifting of the center of shear stresses, from the center of the circular section to a rather asymmetric place, on a perpendicular to the crack edge at its middle. This physically causes the coupling and this is common in both configurations. In any case, a fatigue crack should be better in the experiment, but only a saw cut was used (which is easy to be made) to verify the existence of the coupling.

A fast Fourier transform (FFT) gave the amplitude of acceleration as a function of the flexural frequency of the shaft, and the resonance frequencies were calculated from the FFT plot. The resonance frequencies for the experimental shaft are shown in Table 4. At the same time Table 5 presents the analytical resonance frequencies as a function of the crack depth. Note that, until then, the horizontal response was due to the geometric asymmetry of the experimental model with respect to the plane of the excitation, which was the vertical plane. The vibrator machine could not vibrate perfectly in the vertical direction due to manufacturing constraints. This also applied for the model of the beam and the base in Fig. 12, in which the welding joints made the construction not exclusively symmetric to the vertical plane. So, measurements of the horizontal acceleration were expected even without a cut. The differences between the experimental (Table 4) and the analytical (Table 5) eigenfrequencies for an uncracked shaft ($a/D = 0$) exist because the supposedly clamped end was not exclusively clamped due to the welding joint. Also, the base could not be so stiff as to exclude all horizontal revolution when it was vibrated. The torsion in the clamped end generated a revolution of the base in the vertical plane as shown in Fig. 12. These phenomena could be modeled using torsional springs (vertical and horizontal) in the clamped end as shown in Fig. 14.

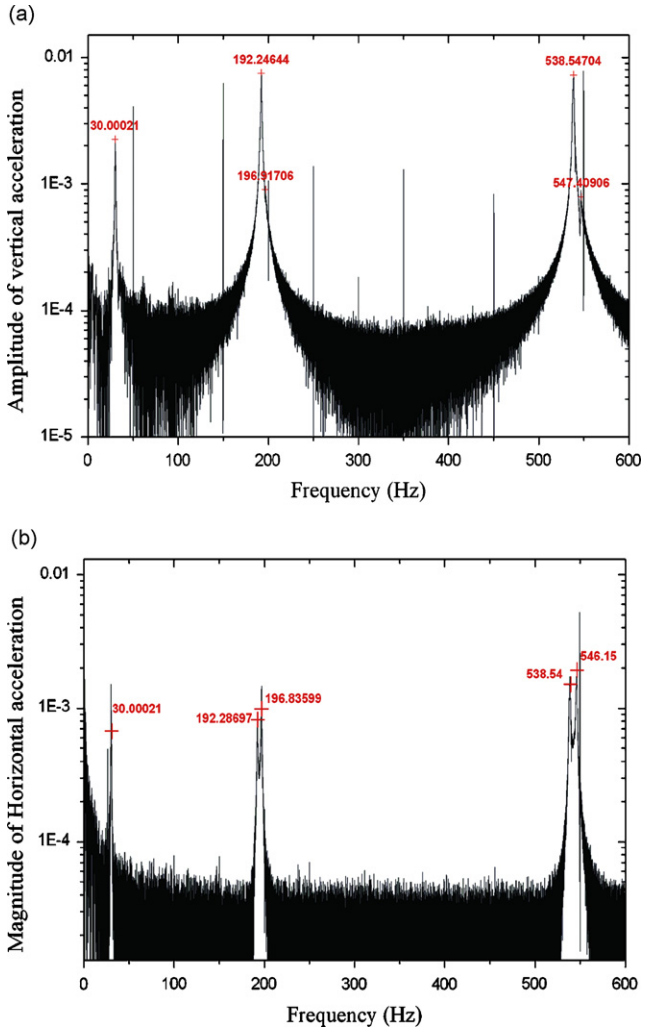

Fig. 15. FFT for (a) vertical and (b) horizontal acceleration of the free end of the shaft without cut in the region of 0–600 Hz.

In this case, the boundary conditions in the clamped end become $Y_1''(0)-K_tY_1'(0)=(0)$ and $Z_1''(0)-K_tZ_1'(0)=(0)$. K_t is the stiffness of the torsional spring in the vertical and horizontal direction. When K_t takes values towards infinity, the model agrees with the analytical one of Section 3. With the new boundary conditions, the characteristic determinant $\det|\mathbf{P}|$ is a function of the frequency ω and of the stiffness K_t. It is feasible to estimate the values of K_t so as to match the analytical eigenfrequencies to the experimental resonance frequencies for the intact case. The FFT plots, of the vertical and horizontal time response, of the intact experimental shaft are shown in Figs. 15a and b. The first three frequencies of the resonance in both directions are presented in Table 4.

By setting, in the matrix $\mathbf{P}$, all local compliances equal to zero (no crack) and $\omega=188.49\,\mathrm{rad\,s^{-1}}$ (first experimental resonance frequency), the equation $\det(\mathbf{P})|_{\omega\,=\,188.5}=0$ gives the value of $K_t=962.2\,\mathrm{N\,m\,rad^{-1}}$. In Table 5, the first three analytical eigenfrequencies for both planes are presented.

In the shaft of Fig. 12, a cut was made with a variable dimensionless depth $\bar{a}=0.2,\ 0.4,\ 0.8$ and $\varphi=90^\circ$; the signals for the vertical and horizontal acceleration were acquired. In Figs. 16a and b, the FFT is plotted, for the vertical and horizontal response, when $\bar{a}=0.8$.

The analytical model considers one crack so as to remain comparable with the experimental one (one cut). In the mathematical model, then, one crack is at $L_1=0.2L$ and the other one is at the free end, where $L_2=L$, so as to have no effect on the vibration. The frequency response is calculated for variable crack depths $\bar{a}=0.2,\ 0.4,\ 0.8$ and $\varphi=90^\circ$. Note that, in order for the coupling peaks to become visible, the excitation frequency

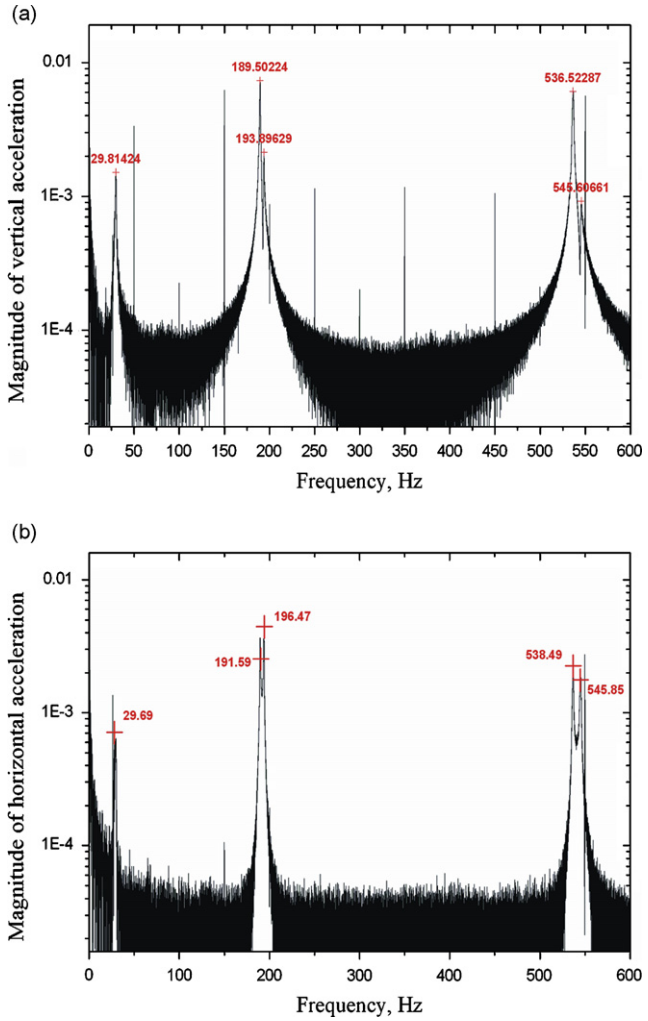

Fig. 16. FFT for (a) vertical and (b) horizontal acceleration of the free end of the cut shaft with a cut of $\bar{a} = 0.8$ in the region of 0–600 Hz.

changes with a step of 10^{-9} in the regions where coupling exists. In the other regions of excitation frequency, the step is equal to 10^{-3}; this is obligatory for procedure endurance. In Figs. 17a and b, the frequency response is plotted for relative crack depth $\bar{a} = 0.8$, for the vertical and horizontal response, respectively.

In Table 4 the double peak measurements, due to the vibration coupling, in the two main bending directions are presented. It can be seen that as the depth of the cut increases, the resonance frequencies in the vertical direction decrease. This is expected, because the deeper cut decreases the shaft stiffness. Note that in the case of the intact experimental shaft, the additional peak of the horizontal response in the vertical response is quite faint, but as the cut depth increases, the additional peak, from one direction to the other, becomes clearly visible and larger in amplitude. This coupling phenomenon becomes clear, when two neighboring eigenfrequencies exist in the area of the resonance of each direction. Note that exactly equal eigenfrequencies are observed in both planes. The corresponding analytical responses show the same phenomenon.

The uncracked shaft has no horizontal response and, in the vertical response, the observed coupling is stronger as the crack depth increases. The change in analytical eigenfrequencies does not exactly match those of the experimental calculations; this is due to the fact that the dimensionless compliances are computed for the semi-closed crack at the rotational angle of 90°, but the experimental cut does not follow this rule because it is made with a 0.5 mm saw (cut). So, the local compliances in the experiment are much different than those calculated from the stress intensity factors. Besides, the slenderness ratio of a cracked beam is a parameter that affects the reduction of

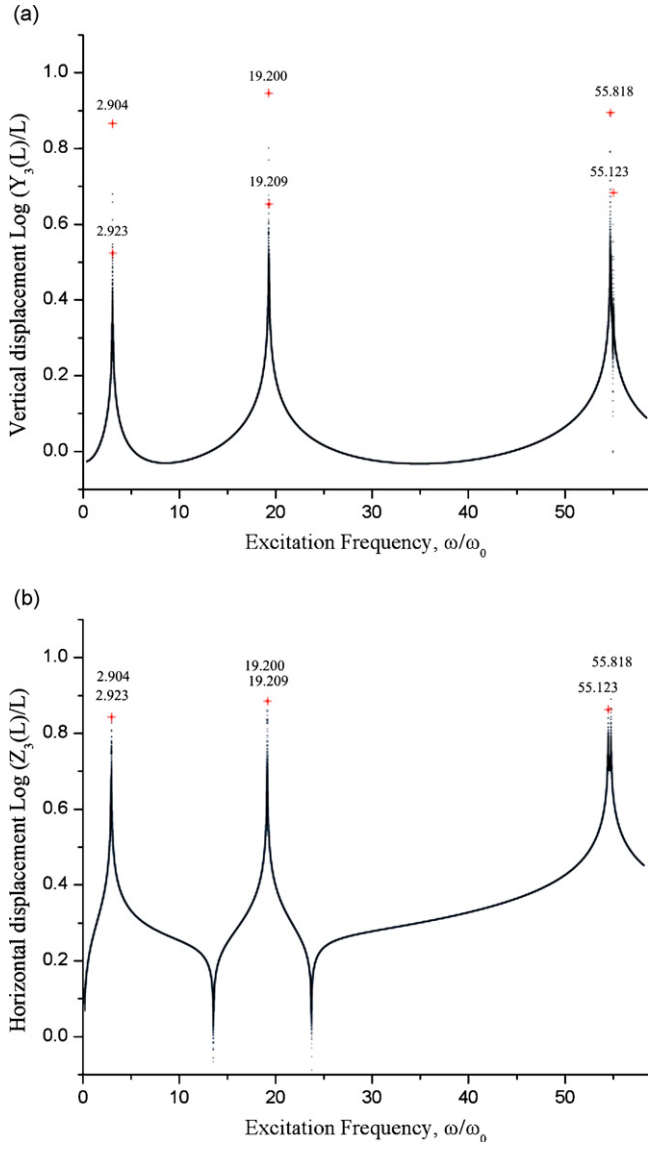

Fig. 17. (a) Vertical and (b) horizontal response of the free end of the cracked shaft with a crack of $\bar{a} = 0.8$.

the eigenfrequencies. Bigger slenderness ratios cause smaller eigenvalue reductions and vise versa [35]. Here the shaft used had a slenderness ratio $\lambda = 2L/R = 2 \times 400/4 = 200$ that is rather big and the reduction of the eigenvalues is not expected to be large. The experimental results are generally repeatable inside a small range of discrepancies.

5. Conclusions

The coupling phenomenon of different vibration modes of a cracked shaft has been reported over the past two decades. This investigation focuses on the coupled bending vibrations, particularly under the presence of two cracks. Even if this kind of coupling in general was known and expected, the past investigations focused on the coupling of longitudinal and bending or on the torsional and bending vibrations. The main conclusions of this investigation could be summarized as follows:

(a) The compliance matrix during the rotation of the crack or of the shaft is computed in every possible rotation angle, and it is not estimated using a small number of computed values. The four

terms of the local compliance matrix were defined supposing that the crack breathes under the effect of gravity.

(b) The frequency response in the analytical and experimental procedures proved that in each spectrum there are resonances in the eigenfrequencies of both planes. In the vertical spectrum, both vertical and horizontal resonances are presented; the same goes for horizontal spectrum. A double peak appears on the vibration spectrum, for a shaft with one or two cracks, indicating the coupling of the vertical and horizontal vibrations. The double peak appears more clearly in both spectrums as the crack depth increases. The fact that two cracks are considered in this paper comes up due to a real situation of high bending moments in a shaft at two different points, as in the case of four points bending of beams.

(c) When the two cracks are in phase, then the coupling phenomenon becomes stronger; meanwhile, if the two cracks are opposite, then the coupling turns weaker.

(d) The coupled response in the horizontal plane under vertical excitation is maximized when the crack is rotated by 90° in reference to the vertical plane. This is the result of the value of the local coupled compliance, which is maximized at this rotational angle.

(e) The experimental procedure proved that the deeper crack makes the coupling phenomenon more intense. This situation depends, of course, on the relative angular position of the cracks.

The experimental results confirmed the existence of the coupling and of the double peaks. The discrepancies observed from the analytical results are due to the flexibility of the clamped end on the vibration table and the fact that a cut was used in the experimental procedure instead of a real fatigue crack. It has been proven that the cut gives a smaller local compliance than that of a crack. A virtual spring was introduced to model the clamped end in order to bring the experimental measurements into agreement with the analytical ones.

Acknowledgments

The assistance of D. Rizos and N. Chrysochoidis, during the experimental work of this paper, is greatly appreciated.

Appendix A

The sub-matrices of matrix **P** in Eq. (17) are defined as follows:

$$\mathbf{A}=\begin{bmatrix}
1 & 0 & 1 & 0 & 0 & 0 & 0 & 0 & 0 & 0 & 0 & 0\\
0 & k_y & 0 & k_y & 0 & 0 & 0 & 0 & 0 & 0 & 0 & 0\\
0 & 0 & 0 & 0 & 0 & 0 & 0 & 0 & k_y^2 ch_{Ly} & k_y^2 sh_{Ly} & -k_y^2 c_{Ly} & -k_y^2 s_{Ly}\\
0 & 0 & 0 & 0 & 0 & 0 & 0 & 0 & k_y^3 sh_{Ly} & k_y^3 ch_{Ly} & k_y^3 s_{Ly} & -k_y^3 c_{Ly}\\
ch_{L_{1y}} & sh_{L_{1y}} & c_{L_{1y}} & s_{L_{1y}} & -ch_{L_{1y}} & -sh_{L_{1y}} & -c_{L_{1y}} & -s_{L_{1y}} & 0 & 0 & 0 & 0\\
k_y^2 ch_{L_{1y}} & k_y^2 sh_{L_{1y}} & -k_y^2 c_{L_{1y}} & -k_y^2 s_{L_{1y}} & -k_y^2 ch_{L_{1y}} & -k_y^2 sh_{L_{1y}} & k_y^2 c_{L_{1y}} & k_y^2 s_{L_{1y}} & 0 & 0 & 0 & 0\\
k_y^3 sh_{L_{1y}} & k_y^3 ch_{L_{1y}} & k_y^3 s_{L_{1y}} & -k_y^3 c_{L_{1y}} & -k_y^3 sh_{L_{1y}} & -k_y^3 ch_{L_{1y}} & -k_y^3 s_{L_{1y}} & k_y^3 c_{L_{1y}} & 0 & 0 & 0 & 0\\
O_{8,1} & O_{8,2} & O_{8,3} & O_{8,4} & O_{8,5} & O_{8,6} & O_{8,7} & O_{8,8} & 0 & 0 & 0 & 0\\
0 & 0 & 0 & 0 & ch_{L_{2y}} & sh_{L_{2y}} & c_{L_{2y}} & s_{L_{2y}} & -ch_{L_{2y}} & -sh_{L_{2y}} & -c_{L_{2y}} & -s_{L_{2y}}\\
0 & 0 & 0 & 0 & -k_y^2 ch_{L_{2y}} & -k_y^2 sh_{L_{2y}} & k_y^2 c_{L_{2y}} & k_y^2 s_{L_{2y}} & k_y^2 ch_{L_{2y}} & k_y^2 sh_{L_{2y}} & -k_y^2 c_{L_{2y}} & -k_y^2 s_{L_{2y}}\\
0 & 0 & 0 & 0 & -k_y^3 sh_{L_{2y}} & -k_y^3 ch_{L_{2y}} & -k_y^3 s_{L_{2y}} & k_y^3 c_{L_{2y}} & k_y^3 sh_{L_{2y}} & k_y^3 ch_{L_{2y}} & k_y^3 s_{L_{2y}} & -k_y^3 c_{L_{2y}}\\
0 & 0 & 0 & 0 & O_{12,5} & O_{12,6} & O_{12,7} & O_{12,8} & -k_y sh_{L_{2y}} & -k_y ch_{L_{2y}} & k_y s_{L_{2y}} & -k_y c_{L_{2y}}
\end{bmatrix},$$

$$\mathbf{B}=\begin{bmatrix} 0 & 0 & 0 & 0 & 0 & 0 & 0 & 0 & 0 & 0 & 0 & 0\\ 0 & 0 & 0 & 0 & 0 & 0 & 0 & 0 & 0 & 0 & 0 & 0\\ 0 & 0 & 0 & 0 & 0 & 0 & 0 & 0 & 0 & 0 & 0 & 0\\ 0 & 0 & 0 & 0 & 0 & 0 & 0 & 0 & 0 & 0 & 0 & 0\\ 0 & 0 & 0 & 0 & 0 & 0 & 0 & 0 & 0 & 0 & 0 & 0\\ 0 & 0 & 0 & 0 & 0 & 0 & 0 & 0 & 0 & 0 & 0 & 0\\ 0 & 0 & 0 & 0 & 0 & 0 & 0 & 0 & 0 & 0 & 0 & 0\\ O_{8,13} & O_{8,14} & O_{8,15} & O_{8,16} & 0 & 0 & 0 & 0 & 0 & 0 & 0 & 0\\ 0 & 0 & 0 & 0 & 0 & 0 & 0 & 0 & 0 & 0 & 0 & 0\\ 0 & 0 & 0 & 0 & 0 & 0 & 0 & 0 & 0 & 0 & 0 & 0\\ 0 & 0 & 0 & 0 & 0 & 0 & 0 & 0 & 0 & 0 & 0 & 0\\ 0 & 0 & 0 & 0 & O_{12,17} & O_{12,18} & O_{12,19} & O_{12,20} & 0 & 0 & 0 & 0 \end{bmatrix},$$

$$\mathbf{C}=\begin{bmatrix} 0 & 0 & 0 & 0 & 0 & 0 & 0 & 0 & 0 & 0 & 0 & 0\\ 0 & 0 & 0 & 0 & 0 & 0 & 0 & 0 & 0 & 0 & 0 & 0\\ 0 & 0 & 0 & 0 & 0 & 0 & 0 & 0 & 0 & 0 & 0 & 0\\ 0 & 0 & 0 & 0 & 0 & 0 & 0 & 0 & 0 & 0 & 0 & 0\\ 0 & 0 & 0 & 0 & 0 & 0 & 0 & 0 & 0 & 0 & 0 & 0\\ 0 & 0 & 0 & 0 & 0 & 0 & 0 & 0 & 0 & 0 & 0 & 0\\ 0 & 0 & 0 & 0 & 0 & 0 & 0 & 0 & 0 & 0 & 0 & 0\\ O_{20,1} & O_{20,2} & O_{20,3} & O_{20,4} & 0 & 0 & 0 & 0 & 0 & 0 & 0 & 0\\ 0 & 0 & 0 & 0 & 0 & 0 & 0 & 0 & 0 & 0 & 0 & 0\\ 0 & 0 & 0 & 0 & 0 & 0 & 0 & 0 & 0 & 0 & 0 & 0\\ 0 & 0 & 0 & 0 & 0 & 0 & 0 & 0 & 0 & 0 & 0 & 0\\ 0 & 0 & 0 & 0 & O_{24,5} & O_{24,6} & O_{24,7} & O_{24,8} & 0 & 0 & 0 & 0 \end{bmatrix},$$

$$\mathbf{D}=\begin{bmatrix} 1 & 0 & 1 & 0 & 0 & 0 & 0 & 0 & 0 & 0 & 0 & 0\\ 0 & k_z & 0 & k_z & 0 & 0 & 0 & 0 & 0 & 0 & 0 & 0\\ 0 & 0 & 0 & 0 & 0 & 0 & 0 & 0 & k_z^2 ch_{Lz} & k_z^2 sh_{Lz} & -k_z^2 c_{Lz} & -k_z^2 s_{Lz}\\ 0 & 0 & 0 & 0 & 0 & 0 & 0 & 0 & k_z^3 sh_{Lz} & k_z^3 ch_{Lz} & k_z^3 s_{Lz} & -k_z^3 c_{Lz}\\ ch_{L_{1z}} & sh_{L_{1z}} & c_{L_{1z}} & s_{L_{1z}} & -ch_{L_{1z}} & -sh_{L_{1z}} & -c_{L_{1z}} & -s_{L_{1z}} & 0 & 0 & 0 & 0\\ k_z^2 ch_{L_{1z}} & k_z^2 sh_{L_{1z}} & -k_z^2 c_{L_{1z}} & -k_z^2 s_{L_{1z}} & -k_z^2 ch_{L_{1z}} & -k_z^2 sh_{L_{1z}} & k_z^2 c_{L_{1z}} & k_z^2 s_{L_{1z}} & 0 & 0 & 0 & 0\\ k_z^3 sh_{L_{1z}} & k_z^3 ch_{L_{1z}} & k_z^3 s_{L_{1z}} & -k_z^3 c_{L_{1z}} & -k_z^3 sh_{L_{1z}} & -k_z^3 ch_{L_{1z}} & -k_z^3 s_{L_{1z}} & k_z^3 c_{L_{1z}} & 0 & 0 & 0 & 0\\ O_{20,13} & O_{20,14} & O_{20,15} & O_{20,16} & O_{20,17} & O_{20,18} & O_{20,19} & O_{20,20} & 0 & 0 & 0 & 0\\ 0 & 0 & 0 & 0 & ch_{L_{2z}} & sh_{L_{2z}} & c_{L_{2z}} & s_{L_{2z}} & -ch_{L_{2z}} & -sh_{L_{2z}} & -c_{L_{2z}} & -s_{L_{2z}}\\ 0 & 0 & 0 & 0 & -k_z^2 ch_{L_{2z}} & -k_z^2 sh_{L_{2z}} & k_z^2 c_{L_{2z}} & k_z^2 s_{L_{2z}} & k_z^2 ch_{L_{2z}} & k_z^2 sh_{L_{2z}} & -k_z^2 c_{L_{2z}} & -k_z^2 s_{L_{2z}}\\ 0 & 0 & 0 & 0 & -k_z^3 sh_{L_{2z}} & -k_z^3 ch_{L_{2z}} & -k_z^3 s_{L_{2z}} & k_z^3 c_{L_{2z}} & k_z^3 sh_{L_{2z}} & k_z^3 ch_{L_{2z}} & s_{L_{2z}} & -k_z^3 c_{L_{2z}}\\ 0 & 0 & 0 & 0 & O_{24,17} & O_{24,18} & O_{24,19} & O_{24,20} & O_{24,21} & O_{24,22} & O_{24,23} & O_{24,24} \end{bmatrix}.$$

Here

$$\begin{array}{llll}
\cosh(k_yL)=ch_{Ly}, & \sinh(k_yL)=sh_{Ly}, & \cos(k_yL)=c_{Ly}, & \sin(k_yL)=s_{Ly},\\
\cosh(k_yL_1)=ch_{L_{1y}}, & \sinh(k_yL_1)=sh_{L_{1y}}, & \cos(k_yL_1)=c_{L_{1y}}, & \sin(k_yL_1)=s_{L_{1y}},\\
\cosh(k_yL_2)=ch_{L_{2y}}, & \sinh(k_yL_2)=sh_{L_{2y}}, & \cos(k_yL_2)=c_{L_{2y}}, & \sin(k_yL_2)=s_{L_{2y}},\\
\cosh(k_zL)=ch_{Lz}, & \sinh(k_zL)=sh_{Lz}, & \cos(k_zL)=c_{Lz}, & \sin(k_zL)=s_{Lz},\\
\cosh(k_zL_1)=ch_{L_{1z}}, & \sinh(k_zL_1)=sh_{L_{1z}}, & \cos(k_zL_1)=c_{L_{1z}}, & \sin(k_zL_1)=s_{L_{1z}},\\
\cosh(k_zL_2)=ch_{L_{2z}}, & \sinh(k_zL_2)=sh_{L_{2z}}, & \cos(k_zL_2)=c_{L_{2z}}, & \sin(k_zL_2)=s_{L_{2z}}
\end{array}$$

and

$$\begin{array}{llll}
O_{8,1}=EIk_y^2ch_{L_{1y}}c_{55_1}+k_ysh_{L_{1y}}, & O_{8,2}=EIk_y^2sh_{L_{1y}}c_{55_1}+k_ych_{L_{1y}}, & O_{8,3}=-EIk_y^2c_{L_{1y}}c_{55_1}-k_ys_{L_{1y}}, & O_{8,4}=-EIk_y^2s_{L_{1y}}c_{55_1}+k_yc_{L_{1y}},\\
O_{8,5}=-k_ysh_{L_{1y}}, & O_{8,6}=-k_ych_{L_{1y}}, & O_{8,7}=k_ys_{L_{1y}}, & O_{8,8}=-k_yc_{L_{1y}},\\
O_{8,13}=EIk_z^2ch_{L_{1z}}c_{54_1}, & O_{8,14}=EIk_z^2sh_{L_{1z}}c_{54_1}, & O_{8,15}=-EIk_z^2c_{L_{1z}}c_{54_1}, & O_{8,16}=-EIk_z^2s_{L_{1z}}c_{54_1},\\
O_{12,5}=EIk_y^2ch_{L_{2y}}c_{55_2}+k_ysh_{L_{2y}}, & O_{12,6}=EIk_y^2sh_{L_{2y}}c_{55_2}+k_ych_{L_{2y}}, & O_{12,7}=-EIk_y^2c_{L_{2y}}c_{55_2}-k_ys_{L_{2y}}, & O_{12,8}=-EIk_y^2s_{L_{2y}}c_{55_2}+k_yc_{L_{2y}},\\
O_{12,17}=EIk_z^2ch_{L_{2z}}c_{54_2}, & O_{12,18}=EIk_z^2sh_{L_{2z}}c_{54_2}, & O_{12,19}=-EIk_z^2c_{L_{2z}}c_{54_2}, & O_{12,20}=-EIk_z^2s_{L_{2z}}c_{54_2},\\
O_{20,1}=EIk_y^2ch_{L_{1y}}c_{45_1}, & O_{20,2}=EIk_y^2sh_{L_{1y}}c_{45_1}, & O_{20,3}=-EIk_y^2c_{L_{1y}}c_{45_1}, & O_{20,4}=-EIk_y^2s_{L_{1y}}c_{45_1},\\
O_{20,13}=EIk_z^2ch_{L_{1y}}c_{44_1}+k_zsh_{L_{1z}}, & O_{20,14}=EIk_z^2sh_{L_{1y}}c_{44_1}+k_zch_{L_{1z}}, & O_{20,15}=-EIk_z^2c_{L_{1y}}c_{44_1}-k_zs_{L_{1z}}, & O_{20,16}=-EIk_z^2s_{L_{1y}}c_{44_1}+k_zc_{L_{1z}},\\
O_{20,17}=-k_zsh_{L_{1z}}, & O_{20,18}=-k_zch_{L_{1z}}, & O_{20,19}=k_zs_{L_{1z}}, & O_{20,20}=-k_zc_{L_{1z}},\\
O_{24,5}=EIk_y^2ch_{L_{2y}}c_{45_2}, & O_{24,6}=EIk_y^2sh_{L_{2y}}c_{45_2}, & O_{24,7}=-EIk_y^2c_{L_{2y}}c_{45_2}, & O_{24,8}=-EIk_y^2s_{L_{2y}}c_{45_2},\\
O_{24,17}=EIk_z^2ch_{L_{2y}}c_{44_2}+k_zsh_{L_{2z}}, & O_{24,18}=EIk_z^2sh_{L_{2y}}c_{44_2}+k_zch_{L_{2z}}, & O_{24,19}=-EIk_z^2c_{L_{2y}}c_{44_2}-k_zs_{L_{2z}}, & O_{24,20}=-EIk_z^2s_{L_{2y}}c_{44_2}+k_zc_{L_{2z}},\\
O_{24,21}=-k_zsh_{L_{2z}}, & O_{24,22}=-k_zch_{L_{2z}}, & O_{24,23}=k_zs_{L_{2z}}, & O_{24,24}=-k_zc_{L_{2z}}.
\end{array}$$

References

[1] A.D. Dimarogonas, S.A. Paipetis, *Analytical Methods in Rotor Dynamics*, Applied Science Publishers, London, 1983.

[2] C.A. Papadopoulos, A.D. Dimarogonas, Coupled longitudinal and bending vibrations of a rotating shaft with an open crack, *Journal of Sound and Vibration* 117 (1) (1987) 81–93.

[3] C.A. Papadopoulos, Coupled vibrations of cracked shafts. 〈http://thesis.Ekt.gr/0551〉, 1987, pp. 1–235 (in Greek).

[4] H. Tada, P.C. Paris, G.R. Irwin, *The Stress Analysis of Cracks Handbook, Paris Productions*, Del Research Corporation, Pennsylvania, 1973.

[5] H. Okamura, H.W. Liu, C. Chu, A cracked column under compression, *Engineering Fracture Mechanics* 1 (3) (1969) 547–564.

[6] H. Liebowitz, H. Vanderveldt, D.W. Harris, Carrying capacity of notched columns, *International Journal of Solids and Structures* 3 (4) (1967) 489–490.

[7] H. Liebowitz, W.D. Claus, Failure of notched columns with fixed ends, *International Journal of Solids and Structures* 5 (9) (1969) 941–950.

[8] J.R. Rice, N. Levy, The part-through a surface crack transversing an elastic plate, *Journal of Applied Mechanics* 39 (1972) 185–194.

[9] A. Dimarogonas, G. Massouros, Torsional vibration of a shaft with a circumferential crack, *Engineering Fracture Mechanics* 15 (3–4) (1981) 439–444.

[10] A.K. Darpe, K. Gupta, A. Chawla, Coupled bending, longitudinal and torsional vibrations of a cracked rotor, *Journal of Sound and Vibration* 269 (1–2) (2004) 33–60.

[11] B. Grabowski, Vibrational behavior of a turbine rotor containing a transverse crack, *Journal of Mechanical Design-Transactions of the ASME* 102 (1) (1980) 140–146.

[12] R. Gasch, Dynamic behavior of a simple rotor with a cross sectional crack, IMechE Conference Publications in Rotating Machinery, Paper No. C178/76, 1976.

[13] H.D. Nelson, C. Nataraj, The dynamics of a rotor system with a cracked shaft, *Journal of Vibration Acoustics Stress and Reliability in Design-Transactions of the ASME* 108 (2) (1986) 189–196.

[14] I.W. Mayes, W.G.R. Davies, A Method of calculating the vibrational behavior of coupled rotating shafts containing a transverse crack, IMechE Conference, Vibration in Rotating Machinery, Paper No. C254/80, 1980.

[15] C.A. Papadopoulos, A.D. Dimarogonas, Stability of cracked rotors in the coupled vibration mode, *ASME, Rotating Machinery Dynamics, 11th Biennial Conference on Mechanical Vibration and Noise*, Boston, Vol. 2, 1987, pp. 25–34.

[16] A.D. Dimarogonas, C.A. Papadopoulos, Crack detection in turbine rotors, *Proceedings of the Second International Symposium on Transport Phenomena*, Dynamics and Design of Rotating Machinery, Vol. 2, Honolulu, HI, 1988, pp. 286–298.

[17] C.A. Papadopoulos, A.D. Dimarogonas, Diagnosis of Edge Cracks in Rotating Shafts, 4th EPRI Incipient Failure Detection Conference, Predictive Maintenance for the 90s, Philadelphia, PA, 1990.
[18] B.K. Schmalhorst, Numerical simulation of cracked rotor vibrations due to measured crack shapes, Honolulu, *Hemisphere* 2 (1998) 271–285.
[19] C. Li, O. Bernasconi, N. Xenophontidis, Generalized approach to the dynamics of cracked shafts, *Journal of Vibration, Acoustics, Stress and Reliability in Design* 111 (3) (1989) 257–263.
[20] J. Wauer, Modelling and formulation of equations of motion for cracked rotating shafts, *International Journal of Solids and Structures* 26 (8) (1990) 901–914.
[21] W.M. Ostachowicz, M.E. Krawczuk, Coupled torsional and bending vibrations of a rotor with an open crack, *Archive of Applied Mechanics (Ingenieur Archiv)* 62 (3) (1992) 191–201.
[22] A.S. Sekhar, B.S. Prabhu, Vibration and stress fluctuation in cracked shafts, *Journal of Sound and Vibration* 169 (5) (1994) 655–667.
[23] O.N.L. Abraham, J. Brandon, The modelling of the opening and closure of a crack, *Journal of Vibration and Acoustics, Transactions of the ASME* 117 (1995) 370–377.
[24] T.C. Tsai, Y.Z. Wang, The vibration of a multi-crack rotor, *International Journal of Mechanical Sciences* 39 (9) (1997) 1037–1053.
[25] A.S. Sekhar, Vibration characteristics of a cracked rotor with two open cracks, *Journal of Sound and Vibration* 223 (4) (1999) 497–512.
[26] A.K. Darpe, K. Gupta, A. Chawla, Dynamics of a two-crack rotor, *Journal of Sound and Vibration* 259 (3) (2003) 649–675.
[27] A.S. Sekhar, Model-based identification of two cracks in a rotor system, *Mechanical Systems and Signal Processing* 18 (4) (2004) 977–983.
[28] D.P. Patil, S.K. Maiti, Detection of multiple cracks using frequency measurements, *Engineering Fracture Mechanics* 70 (12) (2003) 1553–1572.
[29] C.A. Papadopoulos, Some comments on the calculation of the local flexibility of cracked shafts, *Journal of Sound and Vibration* 278 (4–5) (2004) 1205–1211.
[30] A.C. Chasalevris, C.A. Papadopoulos, Identification of multiple cracks in beams under bending, *Mechanical Systems and Signal Processing* 20 (7) (2006) 1631–1673.
[31] W. Theis, Langs- Und Torsions-Schwingungen Bei Quer Angerissenen Rotoren Untersuchungen Auf Der Grundlage Eines Ribmodells Mit 6 Balkenfreiheitsgraden, *Fortschritt-Berichte VDI* 11 (131) (1990) 1–140.
[32] A.C. Chasalevris, C.A. Papadopoulos, Cross coupled bending vibrations of rotating shaft due to a transverse breathing crack, Seventh IFToMM—Conference on Rotor Dynamics, Vienna, Austria, 2006.
[33] A.J.M.A. Gomez, J.M. Montalvao e Silva, Theoretical and experimental data on crack depth effects in the dynamic behavior of free–free beams, 9 (1991) 274–283.
[34] P. Cawley, R. Ray, Comparison of the natural frequency changes produced by cracks and slots, *Journal of Vibration, Acoustics, Stress and Reliability in Design* 110 (3) (1988) 366–370.
[35] M.L. Kikidis, C.A. Papadopoulos, Slenderness ratio effect on cracked beam, *Journal of Sound and Vibration* 155 (1) (1992) 1–11.